Sigma J Eng Nat Sci, Vol. 43, No. 4, pp. 1179–1196, August, 2025

Sigma Journal of Engineering and Natural Sciences
Web page info: https://sigma.yildiz.edu.tr
DOI: 10.14744/sigma.2024.00110

Research Article

MHD flow and effects of hall current, joule heating, and heat source across a chemically reacting and radiating exponentially stretching sheet in a porous medium

Ankur KUMAR SARMA[1,*], Dipak SARMA[1], Sunmoni MUDOI[1]

[1]*Department of Mathematics, Cotton University, Guwahati, 781001, India*

ARTICLE INFO

Article history
Received: 10 March 2024
Revised: 28 May 2024
Accepted: 17 July 2024

Keywords:
bvp4c; Chemical Reaction; Heat Transfer; Mass Transfer; Porous Medium; Radiation

ABSTRACT

This study investigates how Hall current, Joule heating, and a heat source effect flow, heat, and mass transfer across a chemically reacting exponentially stretching sheet in the presence of radiation and a porous medium in a viscous MHD fluid. Some similarity transformations are used to convert the nonlinear governing partial differential equations (PDEs) to nonlinear ordinary differential equations (ODEs). These nonlinear ODEs are then solved numerically using the MATLAB bvp4c approach. Graphs are used to demonstrate the impacts of numerous flow parameters such as magnetic, porosity, Hall, buoyancy, chemical reaction, and mixed convection parameters. Tables are provided to indicate how the coefficient of skin friction, Nusselt number, and Sherwood number vary when the different parameters are changed. The results are also verified using previously published data. The buoyancy parameter enhances the tangential flow velocity while retarding the cross-flow velocity, temperature profile, and concentration profile. Additionally, the hall parameter improves flow while degrading the concentration profile and temperature. Moreover, when the hall parameter increases, the rate of mass and heat transmission increases. The new results are deemed to be extremely satisfactory when compared to earlier research. This research will have a wide range of applications in various industrial and engineering appliances.

Cite this article as: Kumar Sarma A, Sarma D, Mudoi S. MHD flow and effects of hall current, joule heating, and heat source across a chemically reacting and radiating exponentially stretching sheet in a porous medium. Sigma J Eng Nat Sci 2025;43(4):1179–1196.

INTRODUCTION

Magnetohydrodynamics (MHD) is an interdisciplinary discipline that investigates the behavior of electrically conducting fluids such as plasmas and liquid metals in the presence of magnetic fields. It investigates the complex interactions between fluid motion and magnetic forces, including phenomena such as electric current production and magnetic field induction. MHD possesses applications in a variety of domains, including fusion research, astronomy, geophysics, material processing, and aerospace engineering. MHD, which combines fluid dynamics and electromagnetic principles, provides theoretical insights

***Corresponding author.**
*E-mail address: mth2291004_ankur@cottonuniversity.ac.in

This paper was recommended for publication in revised form by Editor-in-Chief Ahmet Selim Dalkilic

into complicated fluid behavior as well as practical solutions for technological breakthroughs that have the potential to revolutionize energy generation, space exploration, and industrial operations.

Hall current refers to the flow of electric charge caused by the Hall effect, which occurs perpendicular to both an electric and magnetic field. When a conducting material carrying an electric current is exposed to a perpendicular magnetic field, the Lorentz force operates on the moving charges, deflecting them to one side of the conductor. This deflection causes charge to accumulate on one side, generating an electric field that resists the passage of charge. As a result, a secondary electric current, known as the Hall current, runs perpendicular to both the initial current and magnetic field. The Hall current is essential for a variety of applications, including magnetic field measurement [1], semiconductor device characterization [2], and the functioning of certain types of sensors [3] and electronic equipment [4].

In magnetohydrodynamics (MHD), joule heating is the process of creating heat within a conducting fluid (such as plasma or liquid metal) owing to the dissipation of electrical currents in the presence of a magnetic field. When an electrically conducting fluid flows through a magnetic field, it induces electric currents inside itself. These currents encounter resistance as they pass through the fluid, resulting in the conversion of electrical energy into heat. This behavior is most noticeable in plasmas, where the high temperatures and magnetic fields found in fusion experiments or astrophysical settings may produce considerable Joule heating effects. Joule heating in MHD systems can have a significant impact on energy transmission, plasma stability, and overall system performance. Understanding and managing joule heating is critical for improving MHD-based technologies, including fusion reactors, magnetohydrodynamic generators, and space propulsion systems. Efforts to regulate joule heating in MHD systems frequently include measures for reducing electrical resistance, controlling current densities, and mitigating thermal impacts to improve system performance and dependability.

Ali *et al.* [5] explored the effects of Hall current on a vertically stretching sheet. The impact of radiation on MHD Newtonian fluid over an exponentially stretched sheet was studied by Kameswaran *et al.* [6]. The flow and heat transfer along a surface that is stretched exponentially and buried in porous material with a fluctuating surface heat flux were studied by Mandal and Mukhopadhyay [7]. The sequel of varying thermal conductivity and non-uniform heat source/sink on MHD flow and heat transfer across an exponentially stretched sheet in a porous medium saturated with Maxwell fluid were studied by Singh and Agarwal [8]. In a porous media with fluctuating viscosity, Khidir and Sibanda [9] probed MHD mixed convective flow, heat and mass transfer over an exponentially stretched surface, and the Soret and Dufour effects. Jaber [10] investigated on the sequel of Hall current and changing viscosity in presence of radiation via stretched sheet. Gorla *et al.* [11], Hayat *et al.* [12], Eid [13] have investigated on heat source/sink, velocity slip condition and heat generation/absorption impacts on exponentially stretching sheet respectively. Srinivasacharya and Jagadeeshwar [14] studied the consequences of Joule heating and Hall current on an exponentially stretched sheet by usage of Chebyshev pseudo spectral method. Govindarajan and Vijayalakshmi [15] examined the impact of Hall current in a dusty fluid across a saturated permeable sheet. Veera Krishna et al. [16] investigated the sequel of radiation and Hall current when a vertical channel filled with porous media experiences an irregular flow. While accounting for the Hall current, Veera Krishna and Chamkha [17] investigated the sequel of heat generation/absorption and thermo-diffusion on an unstable second-grade fluid flow near an infinite vertical plate via porous media. Sarma and Pandit [18] studied the impacts of Hall current, Soret and rotation collectively via infinitely accelerated vertical plate. Rajput and Kanaujia [19] probed the behaviour of Hall current over a rotating inclined plate. Again, Rajput and Kumar [20] researched on the radiation and Hall current behaviour through a temperature-varying inclined plate. Reddy and Sreedevi [21] delved into the study of nanofluid flow via an inclined plate in occurrence of porous medium and chemical reaction. Goud *et al.* [22] probed the outcomes of Joule heating over a vertical plate with an inclined permeable surface when a chemical reaction is occurring. Sandhya *et al.* [23] probed the heat and mass transfer flow across an inclined plate in presence of radiation and chemical reaction. Vijayaragavan *et al.* [24] worked on the comprehensive study of MHD Casson fluid flow across an tilted plate. Dwivedi and Singh [25-26] indulged themselves into the study of cylindrical flow considering the sequel of Hall current. Jeevitha *et al.* [27] studied flow behaviour via a rotating vertical cone in occurrence of porous medium. In occurrence of Joule heating, Tasnim *et al.* [28] examined the sequel of MHD and entropy creation on a square enclosure filled with nanofluid and equipped with several heat-generating devices. Recently, several researchers [29-37] have considered the effects of hall current on the various fluid flow geometry.

The transmission of heat and mass along an exponentially expanding surface has been the subject of previous research, but the combined sequel of slip and Hall currents in the occurrence of radiation and heat creation via a porous medium has received less attention. In the occurrence of radiation and heat production, together with Hall currents, this article concentrates on a novel study of mixed convection slip flow, heat, and mass transfer over a porous exponentially stretched sheet under suction or injection. We have considered a viscous Newtonian fluid in presence of porous medium using the combination of Brinkman equation with the Navier- Stokes equation

[38,39]. This model of porous medium is known as the Darcy-Brinkman model of porous medium. This investigation has several applications in the fields of engineering, heat exchangers, mixing tanks, fluidized bed reactors [40], polycrystalline semiconductors [41], sensors [3], semiconductor detectors [2], and different electronic equipment [4].

MATHEMATICAL FORMULATION

Consider an incompressible viscous fluid with temperature $T_w(x)$ and concentration $C_w(x)$ flowing continuously over an exponentially stretched sheet via electrical conductivity. The z-axis corresponds with the leading edge of the sheet, the y-axis is perpendicular to the sheet in the outward direction of flow, and the positive x-axis is taken along the sheet in the direction of flow. The distance x from the slit causes an exponential shift in the sheet velocity. It is assumed that temperature and concentration of the ambient medium are T∞ and C∞. An intense magnetic field with strength B(x) is applied in the y direction, taking into account the effects of Hall current. The induced magnetic field is disregarded when a very low magnetic Reynolds number is assumed. This presumption is correct since liquid metals and partially ionized fluids which are frequently used in industrial applications have very low magnetic Reynolds numbers. The cross flow in the z-direction brought on by Hall current›s occurrence makes the flow three dimensional [42]. The concentration and temperature of the plate are denoted by C and T, respectively, whereas the velocity vector is (u, v, w). Figure 1 exhibits the geometrical representation of the flow.

The following equations govern the current flow problem in the case of joule heating under the previously mentioned assumptions, together with Boussinesq and boundary layer approximations [14]:

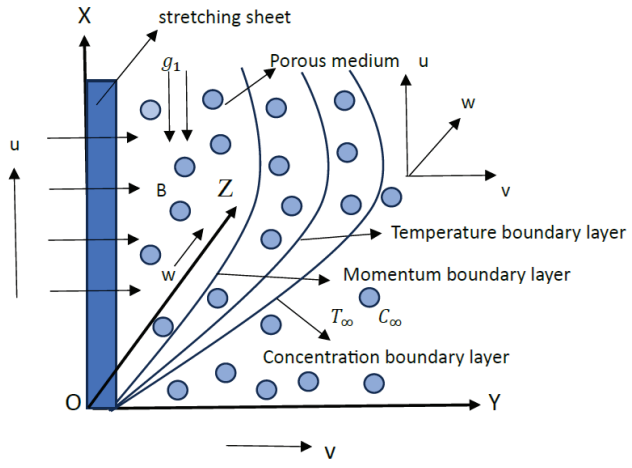

Figure 1. Geometrical representation of the flow problem.

$$\frac{\partial u}{\partial x}+\frac{\partial v}{\partial y}=0 \tag{1}$$

$$u\frac{\partial u}{\partial x}+v\frac{\partial u}{\partial y}=\nu\frac{\partial^2 u}{\partial y^2}+g_1\,\beta_t(T-T_\infty)+g_1\,\beta_c(C-C_\infty)-\frac{\nu}{k_1}u \tag{2}$$

$$u\frac{\partial w}{\partial x}+v\frac{\partial w}{\partial y}=\nu\frac{\partial^2 w}{\partial y^2}+\frac{\sigma B^2}{\rho(1+h^2)}(hu-w)-\frac{\nu}{k_1}w \tag{3}$$

$$u\frac{\partial T}{\partial x}+v\frac{\partial T}{\partial y}=\alpha\frac{\partial^2 T}{\partial y^2}+\frac{\sigma B^2}{\rho C_p(1+h^2)}(u^2+w^2)-\frac{1}{\rho C_p}\frac{\partial q_r}{\partial y}+\frac{Q}{\rho C_p}(T-T_\infty) \tag{4}$$

$$u\frac{\partial C}{\partial x}+v\frac{\partial C}{\partial y}=D\frac{\partial^2 C}{\partial y^2}-K^*(C-C_\infty) \tag{5}$$

The relevant boundary conditions [14] associated with the surface are:

$$u=U(x)+N\nu\frac{\partial u}{\partial y},\quad v=-V(x),\quad w=0 \tag{6}$$

$$T_w=T_\infty+T_0e^{\frac{2x}{L}},\quad C_w=C_\infty+C_0e^{\frac{2x}{L}}\quad \text{at}\quad y=0 \tag{7}$$

$$u\to 0,\quad w\to 0,\quad T\to T_\infty,\quad C\to C_\infty\quad \text{as}\quad y\to\infty \tag{8}$$

Here $B(x)=B_0e^{\frac{x}{2L}}$ is the magnetic field and B_0 is the constant magnetic field, $U(x)=U_0e^{\frac{x}{L}}$ is the stretching velocity, where U_0 is the reference velocity, $V(x)=V_0e^{\frac{x}{2L}}$ is the special velocity at the wall, where V_0 is the initial strength of suction, $N=N_0e^{\frac{-x}{2L}}$ is the velocity slip factor, where in case of no slip, $N=0$

q_r is described as follows

$$q_r=-\frac{4\sigma_1}{3k}\frac{\partial T^4}{\partial y}$$

where σ_1 indicates Stefan-Boltzmann constant and k represents Rosseland mean absorption coefficient.

We presume that the distinction in internal flow temperature is suitably minimal, as shown by the Taylor series expansion about, while ignoring the terms with higher order as,

$$T^4=4T_\infty^3T-3T_\infty^4$$

Now we introduce the similarity transformation [14] and the nondimensional quantities as follows:

$$\eta=\sqrt{\frac{U_0}{2\nu L}}e^{\frac{x}{2L}}y,\ \psi=\sqrt{2\nu LU_0}e^{\frac{x}{2L}}f,\ u=U_0e^{\frac{x}{L}}f',\ v=-\sqrt{\frac{\nu U_0}{2L}}e^{\frac{x}{2L}}(f+\eta f'),$$

$$w=U_0e^{\frac{x}{L}}g,\ T=T_\infty+T_0e^{\frac{2x}{L}}\theta(\eta),\ C_\infty+C_0e^{\frac{2x}{L}}\phi(\eta),\ H=\frac{2L\sigma B_0^2}{\rho U_0},$$

$$\zeta=\frac{Gr}{Re^2},\ Sp=\frac{2\nu L}{k_1U},\ Gr=\frac{g_1\beta_tT_0L^3}{\nu^2},\ Bu=\frac{\beta_cC_0}{\beta_tT_0},\ Pr=\frac{\nu}{\alpha},$$

$$R=\frac{4\sigma_1T_\infty^3}{\kappa k},\ Ec=\frac{U_0^2}{C_pT_0},\ \delta=\frac{2LQ}{\rho C_pU},\ Sc=\frac{\nu}{D},\ K=\frac{2LK^*}{U},\ Re=\frac{U_0L}{\nu}$$

Using the above similarity transformations and nondimensional quantities the PDEqs. (2)-(5) are transformed into the following nonlinear ODEs as follows:

$$f'''+ff''-2f'^2-\frac{H}{(1+h^2)}(f'+hg)+2\zeta(\theta+Bu\phi)-Spf'=0 \quad (9)$$

$$g''-2f'g+g'f+\frac{H}{1+h^2}(hf'-g)-Spg=0 \quad (10)$$

$$\left(1+\frac{4}{3}R\right)\theta''+Pr(\theta'f-4\theta f')+\delta\theta+\frac{HEcPr}{(1+h^2)}(f'^2+g^2)=0 \quad (11)$$

$$\phi''+Sc(f\phi'-4f'\phi)-ScK\phi=0 \quad (12)$$

The boundary conditions (6)-(8) are transformed to the following form:

$$f(0)=S,\ f'(0)=1+\lambda f''(0),\ g(0)=0,\ \theta(0)=1,\ \phi(0)=1, \quad (13)$$

$$f'(\infty)\to 0,\quad g(\infty)\to 0,\quad \theta(\infty)\to 0,\quad \phi(\infty)\to 0 \quad (14)$$

where $S=V_0\sqrt{\frac{2L}{\nu U_0}}$ is the suction/injection as S > 0 or S < 0 respectively, $\lambda=N_0\sqrt{\frac{\nu U_0}{2L}}$ represents the velocity slip parameter.

The expression of the various engineering terms, such as the wall shear stress in x and z- direction, heat and mass transfer rates, respectively are given as follows:

$$\tau_{wx}=\mu(\frac{\partial u}{\partial y})_{y=0},\ \tau_{wz}=\mu(\frac{\partial w}{\partial y})_{y=0},\ q_h=-k(\frac{\partial T}{\partial y})_{y=0},\ \text{and}\ q_m=-D(\frac{\partial C}{\partial y})_{y=0} \quad (15)$$

The local skin friction coefficient along x-direction C_x, local skin friction coefficient along z-direction C_z, local Nusselt number Nu and local Sherwood number Sh are defined as follows:

$$C_x=\frac{2\tau_{wx}}{\rho U^2},\ C_z=\frac{2\tau_{wz}}{\rho U^2},\ Nu=\frac{xq_h}{k(T_w-T_\infty)},\ Sh=\frac{xq_m}{D(C_w-C_\infty)} \quad (16)$$

Using the nondimensional quantities the following results are obtained:

$$f''(0)=\sqrt{\frac{L}{2x}}R_x^{\frac{1}{2}}C_x,\ g'(0)=\sqrt{\frac{L}{2x}}R_x^{\frac{1}{2}}C_z,\ -\theta'(0)=\sqrt{\frac{2L}{x}}R_x^{\frac{-1}{2}}Nu \quad \text{and}\ -\phi'(0)=\sqrt{\frac{2L}{x}}R_x^{\frac{-1}{2}}Sh \quad (17)$$

where $R_x=\frac{xU(x)}{\nu}$ is the local Reynolds number.

MATERIALS AND METHODS

Boundary value problems, either linear or nonlinear, are evaluated using MATLAB solution bvp4c. It can accurately calculate y(x) for each x in [a,b] while taking into consideration the stage-by-stage boundary limitations. This method changes the boundary conditions at infinity to those at a point when it is reasonable to attempt to solve the current issue. The three-stage Lobatto IIIa formula is executed as a finite difference code by bvp4c. Shampine *et al.* [43] suggested this Lobato IIIa approach. This collocation polynomial divides the interval into subintervals based on a mesh of points, providing uniform fourth-order correct solutions across the interval. The solver makes an estimate of the numerical error on each subinterval. If the answer doesn›t satisfy the tolerance requirements, the mesh is adjusted, and the procedure is repeated. However, in addition to the initial mesh points, an initial assumption about the solution at the grid points is unavoidably needed. By adjusting the step size as it goes along and offering a preliminary estimate at the beginning mesh points, the algorithm produces specified precision. Equations (9), (10) and (11) are transformed as follows in order to apply the finite difference-based solver bvp4c:

$$f=y_1, f'=y_1'=y_2, f''=y_2'=y_3, g=y_4, g'=y_5,$$
$$\theta=y_6, \theta'=y_6'=y_7, \phi=y_8, \phi'=y_8'=y_9$$

$$y_3'=-y_1y_3+2y_2^2+\frac{H}{(1+h^2)}(y_2+hy_4)-2\zeta(y_6+Buy_8)+S_py_2 \quad (18)$$

$$y_5'=2y_2y_4-y_5y_1-\frac{H}{(1+h^2)}(hy_2-y_4)+Spy_4 \quad (19)$$

$$y_7'=\frac{1}{\left(1+\frac{4}{3}R\right)}\left[-\frac{HEcPr}{(1+h^2)}(y_2^2+y_4{}^2)-\delta y_6-Pr(y_1y_7-4y_6y_2)\right] \quad (20)$$

$$y_9'=Sc[Ky_8-(y_1y_9-4y_2y_8)] \quad (21)$$

The initial and boundary conditions (10) are transformed as follows:

$$y_1(0)=S,\ y_2(0)=1+\lambda y_3(0),\ y_4(0)=0,\ y_6(0)=1,\ y_8(0)=1 \quad (22)$$

$$y_2(\infty)=0,\ y_4(\infty)=0,\ y_6(\infty)=0,\ y_8(\infty)=0 \quad (23)$$

To satisfy the convergence requirements, the accuracy is measured up to the sixth decimal place. Shampine *et al.* [43] gave the detailed explanation of this scheme. The algorithm of this scheme in given by Figure 2 [44].

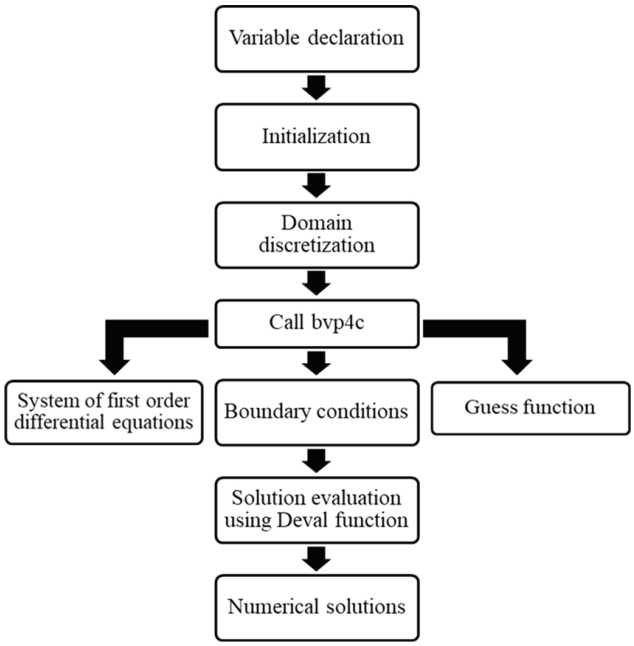

Figure 2. Algorithm of bvp4c. [From Wahid *et al.* [44], with permission from Springer.]

Validation

Table 1 provides a verified example of the correctness and precision of the methodology used in this work. In this instance, the bvp4c approach is applied to compare the outcomes generated by [45] and [14] for $f''(0)$ and $f(\infty)$, disregarding the values of S, λ, ζ and H are shown in Table 1. The approach is dependable since the current study›s calculated results are consistent with the earlier findings.

Additionally, the values of $-\theta'(0)$ for various values of Pr show good agreement with the present results when comparing the equations discussed by Ishak [46] with the current equations. The findings for $-\theta'(0)$ are presumably compared using the bvp4c approach, ignoring the values of S, λ, ζ, Bu, δ, R, H, h, Sp, Sc, Ec and K for varying values of Pr.

RESULTS AND DISCUSSION

Under the aforementioned considerations, the problem is numerically solved, and graphs from Figures. 3 to 33 illustrates the behaviors of tangential flow, cross flow, temperature and concentration for parameters, such as the porosity parameter (Sp), mixed convection parameter (ζ), radiation parameter (R), Magnetic parameter (H), Eckert number (Ec), Hall parameter (h), Bouyancy ratio parameter (Bu), Prandtl number (Pr), heat source (δ), Schmidt number (Sc), and chemical reaction parameter (K). The following standard values for the parameters are taken from [14] as Pr = 0.71, Ec = 0.5, H = 1.0, h = 2.0, Bu = 0.5, ζ = 1, R = 1, Sp = 0.4, Sc = 0.22, K = 1, δ = 1, S = 0.5, and λ = 1.0. Furthermore, variations in skin friction (τ), nusselt number (Nu) and sherwood number (Sh), under various conditions in relation to the different flow parameters are explored and illustrated in Tables 3 and 4.

Tangential Velocity Profile ($f'(\eta)$)

The impact of Bu on $f'(\eta)$ is exhibited in Figure 3. It can be perceived that as Bu rises, $f'(\eta)$ also rises near the sheet, whereas it shows reverse trend as we move away from sheet. The impact of H on $f'(\eta)$ is exhibited in Figure 4. It exhibits that when the value of H escalates, the tangential velocity decreases near the sheet. A homogeneous magnetic field normal to the direction of flow is applied to produce the Lorentz force. The fluid›s velocity in the boundary layer tends to be slowed down by this force. As a result, the tangential velocity decreases as H increases.

Also, it is depicted that the tangential velocity escalates with the rise in H away from the sheet.

Figure 5 shows how the Hall parameter (h) effects $f'(\eta)$. It is perceived from Figure 5 that as h escalates, so does the tangential velocity near the sheet. Effective conductivity decreases with increasing h, and this lowers the magnetic

Table 1. Comparison of $f''(0)$ and $f(\infty)$ with earlier results

	Magyari and Keller [45]	Srinivasacharya and Jagadeeshwar [14]	Present results
$f''(0)$	-1.281808	-1.28180856	-1.2818
$f(\infty)$	0.905639	0.90564383	0.9055

Table 2. Comparison of $-\theta'(0)$ for several values of Pr

Pr	Ishak [46]	Present values
1	0.9548	0.9548
2	1.4715	1.4715
3	1.8691	1.8691

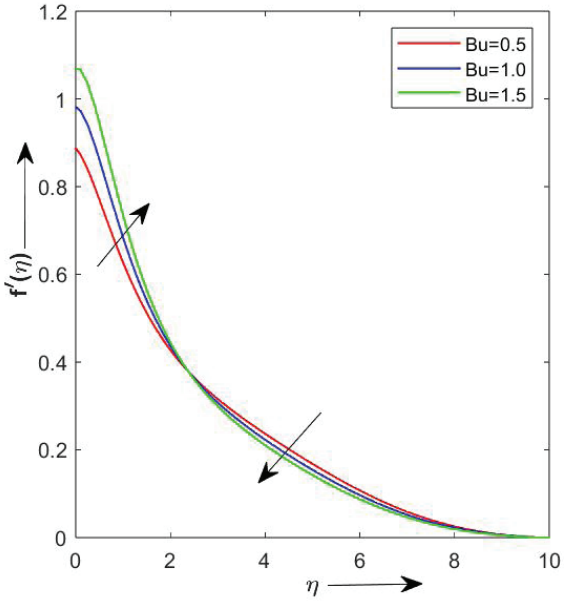

Figure 3. $f'(\eta)$ vs Bu.

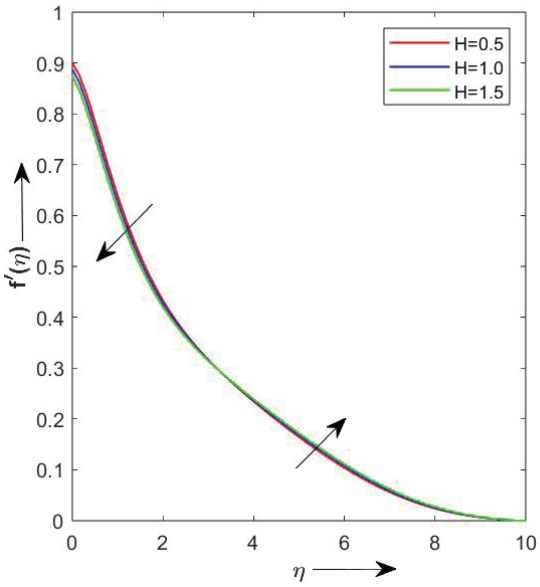

Figure 4. $f'(\eta)$ vs H.

damping force acting on $f'(\eta)$. As a result $f'(\eta)$ rises near the sheet, whereas it decreases as we move away from the sheet. Figure 6 shows the effect on $f'(\eta)$ for higher values of Pr. $f'(\eta)$ decreases as a result of the escalating values of Pr lowering the momentum boundary layer size. Prandtl number indicates how the thermal conductivity is related to the fluid viscosity at reference and the specific heat at constant pressure. Since the viscous forces are too strong to keep the fluid particles securely at constant pressure, $f'(\eta)$ decreases as Pr increases.

The effects of Sp on $f'(\eta)$ are seen in Figure 7. It is discovered that increasing Sp values decreases the velocity profiles and increases the thickness of the velocity boundary layer near the sheet, whereas it shows reverse trend as we move away from the sheet. As the flow resistance escalates in occurrence of porous medium, $f'(\eta)$ reduces. It is evident

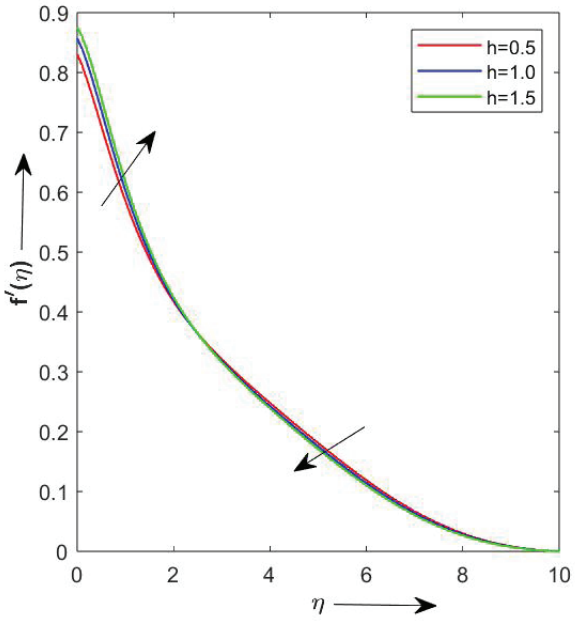

Figure 5. $f'(\eta)$ vs h.

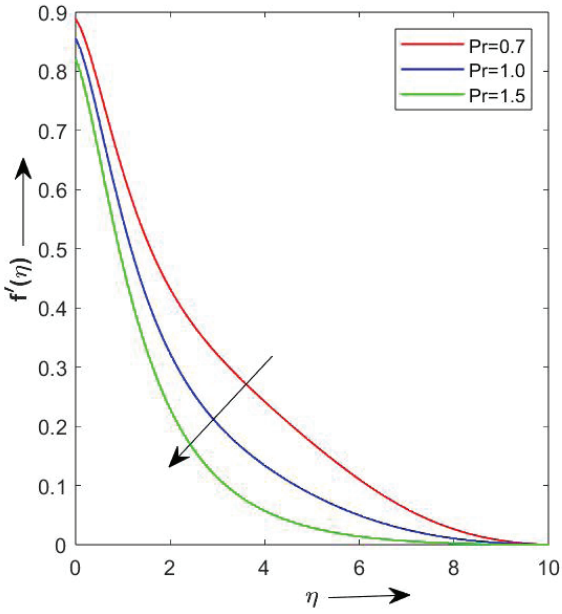

Figure 6. $f'(\eta)$ vs Pr.

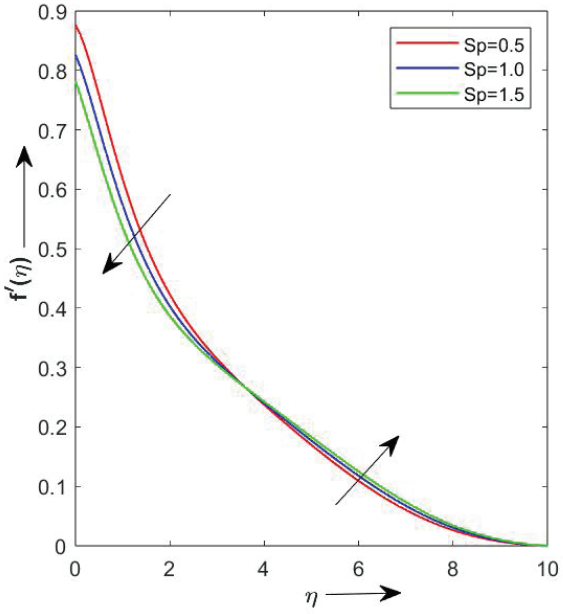

Figure 7. $f'(\eta)$ vs Sp.

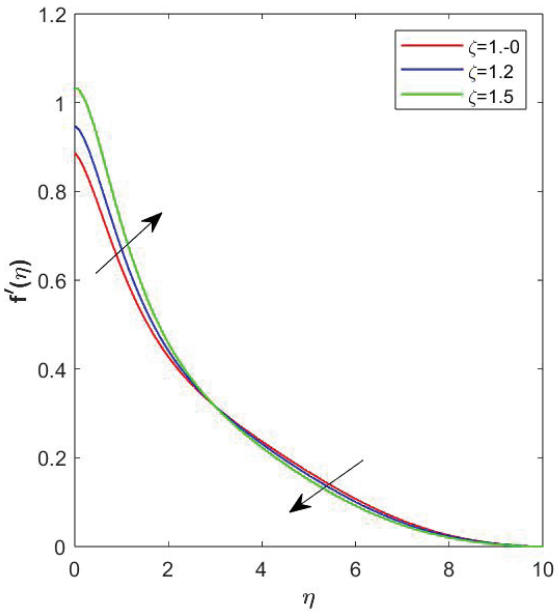

Figure 8. $f'(\eta)$ vs ζ.

from Figure 8 that as the values of ζ grows, so does the tangential velocity near the sheet, whereas it shows reverse trend as we move away from the sheet. This is a result of positive values of ζ create a pressure gradient that is beneficial and enhances the boundary layer fluid flow near the sheet.

Cross Flow Velocity Profile ($g(\eta)$)

The impact of Bu on $g(\eta)$ is exhibited in Figure 9. It can be observed that as Bu rises, $g(\eta)$ decreases away from the sheet. $g(\eta)$ results from the application of a high magnetic field, $g(\eta)$ does not exist in absence of magnetic field (H=0). However, when magnetic field increases, the Hall effect causes a cross flow to automatically form transversely. It also shows that as Bu rises, $g(\eta)$ escalates near the sheet. From Fig. 10, the effect of H on $g(\eta)$ is explored. $g(\eta)$, is produced by a strong applied magnetic field. Figure 10 shows that the $g(\eta)$ increases together with the magnetic field value H. The z-axis direction is where the cross flow

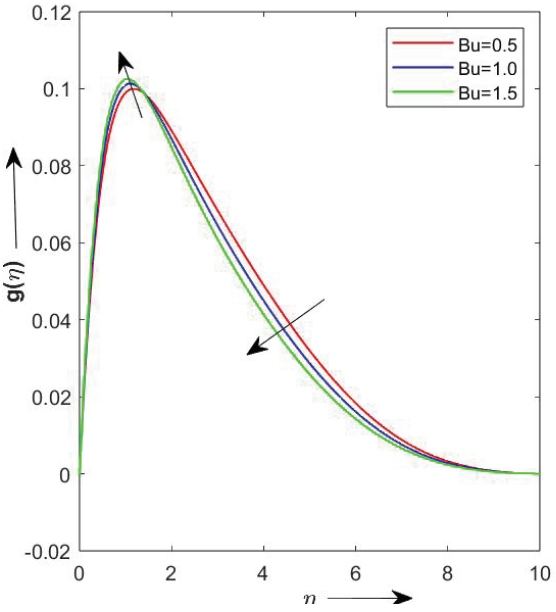

Figure 9. $g(\eta)$ vs Bu.

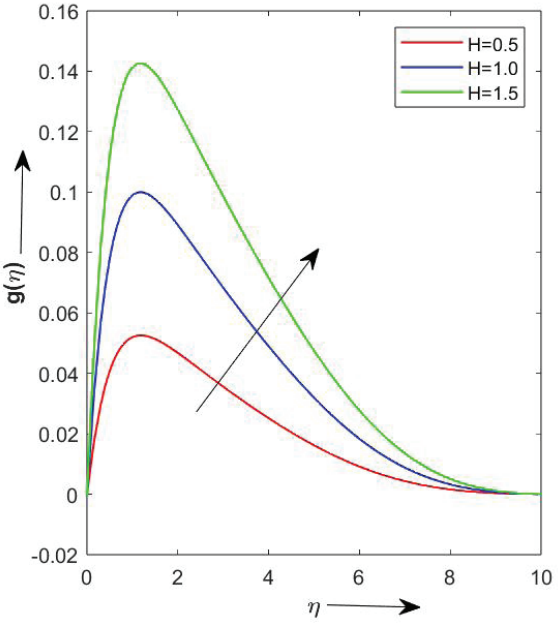

Figure 10. $g(\eta)$ vs H.

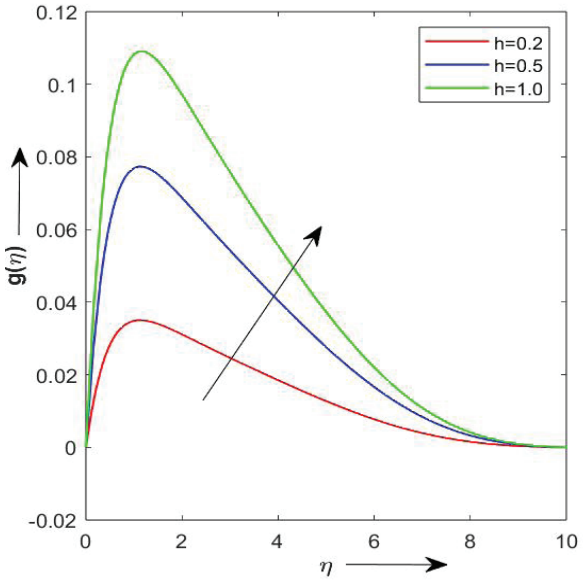

Figure 11. $g(\eta)$ vs h.

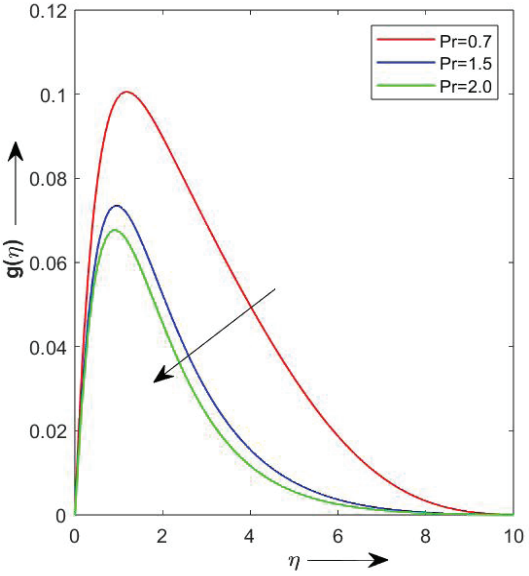

Figure 12. $g(\eta)$ vs Pr.

$g(\eta)$ is induced by the Hall effect. Since the strong magnetic field is applied along the y-axis, which causes the Hall parameter h, the Hall force is parallel to the z-axis and flow rises in the direction of the Hall force.

As illustrated in Figure 11, $g(\eta)$ rises as h increases. Furthermore, with extremely high values of h, the magnetic force terms assume zero, such that the $g(\eta)$ profiles trend to their classical hydrodynamic values as h approaches infinity. The influence of Pr on $g(\eta)$ is shown in Figure 12. The link between the product of fluid viscosity and specific heat and thermal conductivity is established by the Prandtl number under constant pressure using a reference point. $g(\eta)$ decreases with rising values of Pr because under constant pressure, the viscous forces are too strong to retain the fluid particles (atoms/molecules).

Figure 13 shows the impact of Sp on the $g(\eta)$. It is found that when Sp values grow, the VBL thickens and the $g(\eta)$ drops. $g(\eta)$ decreases when the flow resistance rises due to

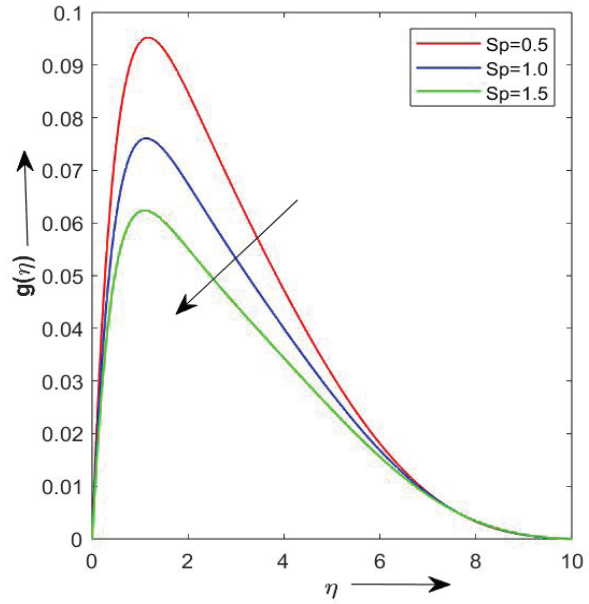

Figure 13. $g(\eta)$ vs Sp.

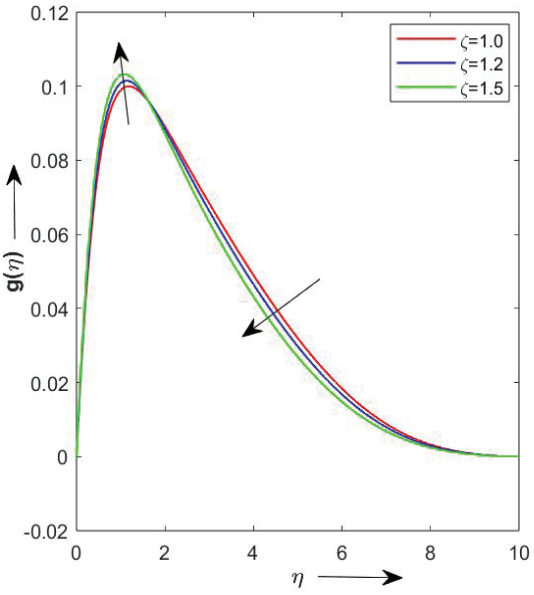

Figure 14. $g(\eta)$ vs ζ.

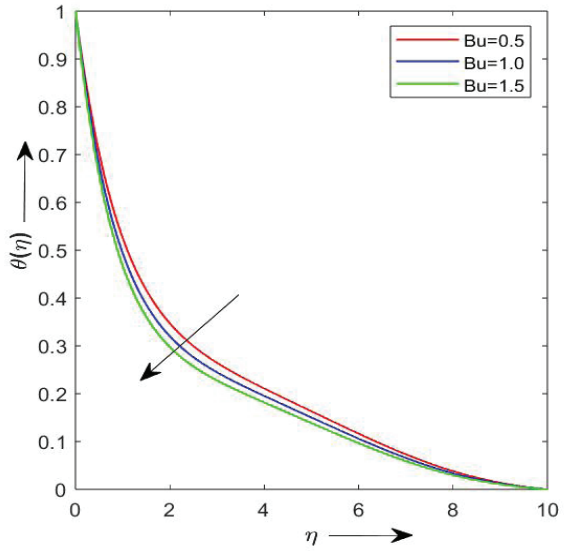

Figure 15. $\theta(\eta)$ vs Bu.

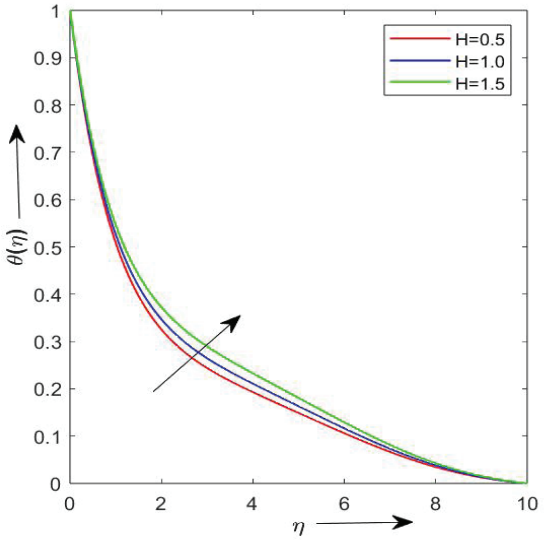

Figure 16. $\theta(\eta)$ w.r.t H.

the presence of porous media. Figure 14 makes it clear that $g(\eta)$, drops as ζ increases away from the sheet. This is due to pressure gradient produced by positive values of ζ, and this gradient lowers $g(\eta)$ away from the sheet. Whereas, it shows reverse trend near the sheet.

Temperature Profile ($\theta(\eta)$)

The impact of Bu on $\theta(\eta)$ is exhibited in Figure 15. It can be observed that as Bu rises, the fluid's temperature decreases. In contrast, the temperature escalates with the rise in H as shown in Figure 16. This is due to the fact that when an electrically charged fluid is exposed to a transverse magnetic field, it gives rise to a resistive force, known as the Lorentz force. By increasing the friction between its layers, this force causes the fluid to encounter resistance. As a result, the temperature in the boundary layer rises.

Figure 17 depicts the sequel of Hall parameter h on $\theta(\eta)$. It is seen that with the rise in h, the fluid's temperature decreases. The sequel of Pr on $\theta(\eta)$ is depicted in Figure 18. It is evident from the graph that temperature $\theta(\eta)$ decreases

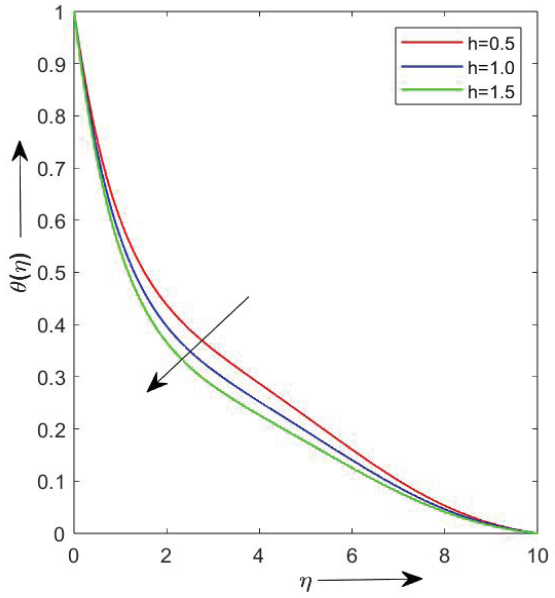

Figure 17. $\theta(\eta)$ vs h.

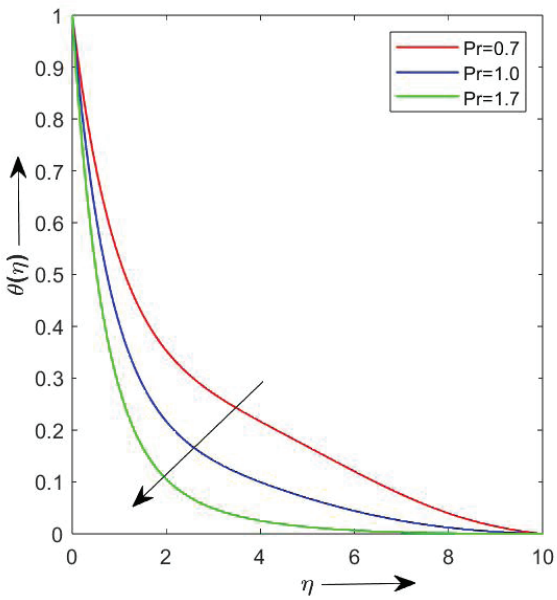

Figure 18. $\theta(\eta)$ vs Pr.

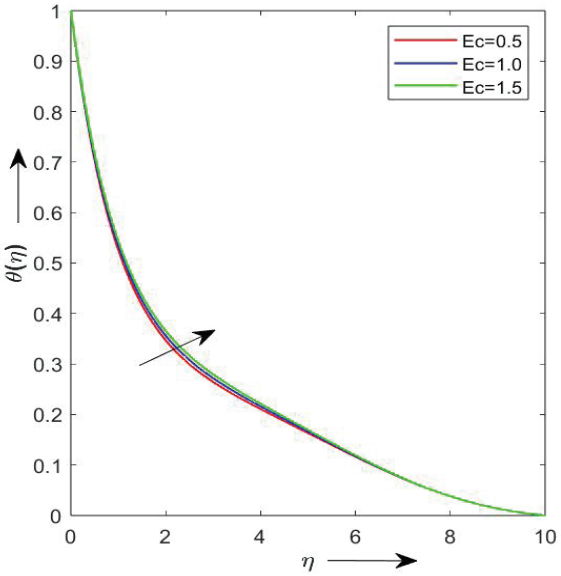

Figure 19. $\theta(\eta)$ vs Ec.

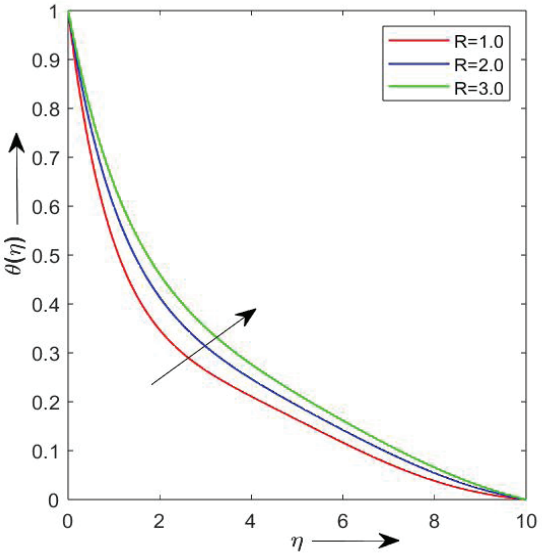

Figure 20. $\theta(\eta)$ vs R.

as Prandtl number Pr increases. Fluids with high Prandtl number have comparatively poor thermal conductivity, which lowers the fluid's temperature by decreasing conduction and TBL size.

The temperature distribution for various Ec values is shown in Figure 19. The temperature distribution $\theta(\eta)$ escalates as Ec rises. This is consistent with the idea that energy is deposited in the fluid zone due to the dissipation caused by viscosity and elastic deformation. As the quantities of thermal radiation parameter R grow, Figure 20 shows that $\theta(\eta)$ increases, leading to an increase in the size of TBL. This is because an escalation in radiation parameter R results in a drop in the mean Roseland absorption co-efficient k, which raises the temperature profile. Radiation usually happens at high temperatures.

Figure 21 exhibits the sequel of δ on $\theta(\eta)$. It can be noticed that as δ escalates, the fluid's temperature escalates, as a result thickens the TBL. Figure 22. depicts the sequel of Sc on $\theta(\eta)$. It exhibits that as Sc increases, the dimensionless temperature $\theta(\eta)$ rises as well, causing the TBL to narrow.

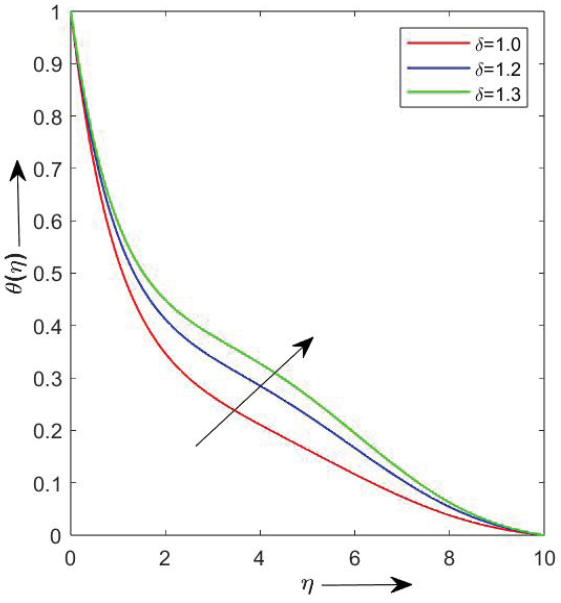

Figure 21. $\theta(\eta)$ vs δ.

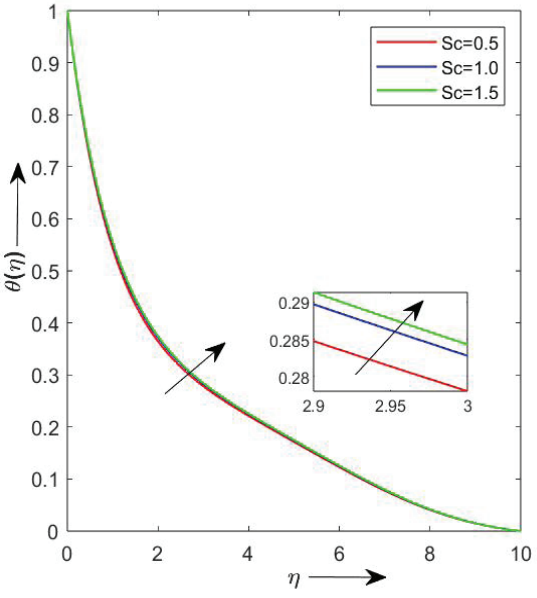

Figure 22. $\theta(\eta)$ w.r.t Sc.

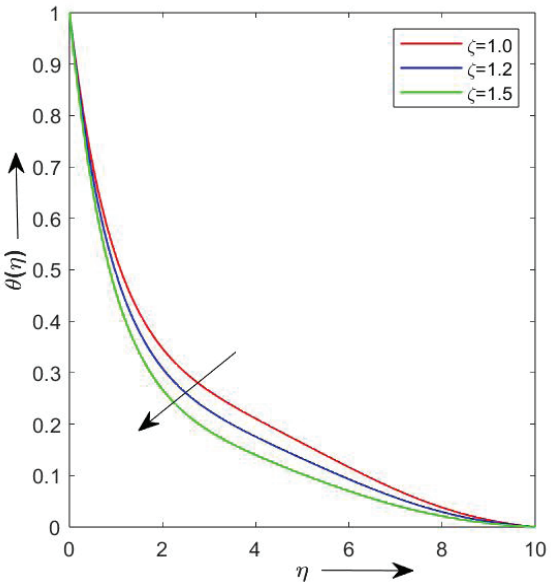

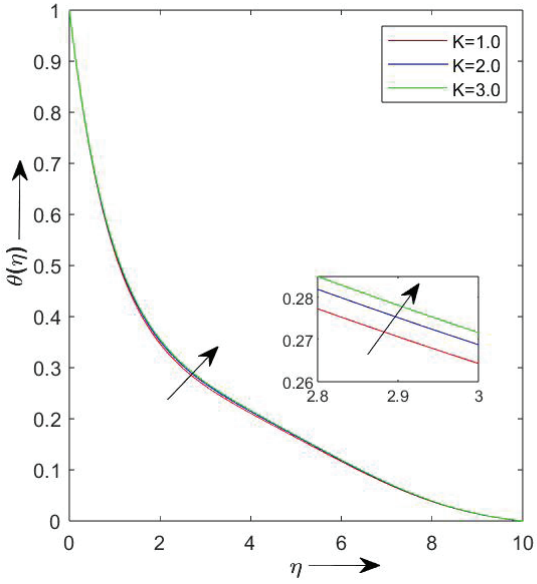

Figure 23. $\theta(\eta)$ vs ζ. **Figure 24**. $\theta(\eta)$ vs K.

It results as an increase in molecular diffusivity causes the fluid molecule's kinetic energy to rise as well, resulting in an increase in average speed and range of motion. The fluid›s temperature escalates as a result.

It can be observed from Figure 23 that when ζ values increase, the temperature drops. This can be attributed to the fluid›s acceleration caused by positive values of ζ, which lowers the TBL. From Figure 24 it can be noticed that as K increases, the fluid's temperature escalates.

Concentration Profile ($\phi(\eta)$)

The impact of Bu on $\phi(\eta)$. is exhibited in Figure 25. It can be perceived that as Bu rises, the fluid's concentration declines. Figure 26 shows the effect of H on $\phi(\eta)$. The concentration field $\phi(\eta)$ rises with escalating values of H, indicating that the magnetic field regulates the fluid flow. The strong magnetic field induces the Lorentz force, which regulates the fluid flow.

Figure 27 depicts the effect of h on $\phi(\eta)$.$\phi(\eta)$ is not favoured by the Hall effect, meaning that concentration

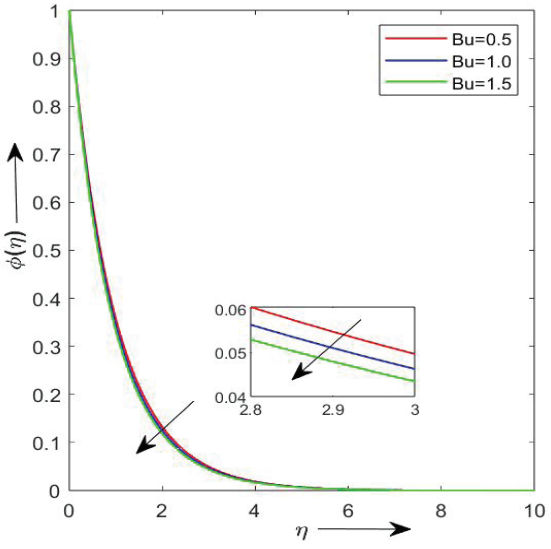

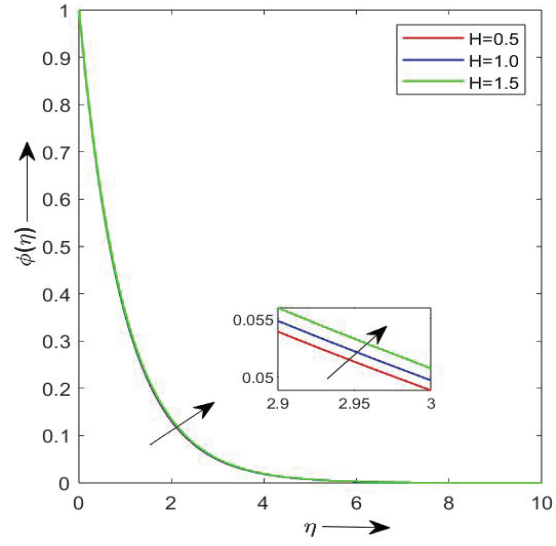

Figure 25. $\phi(\eta)$ vs Bu.

Figure 26. $\phi(\eta)$ vs H.

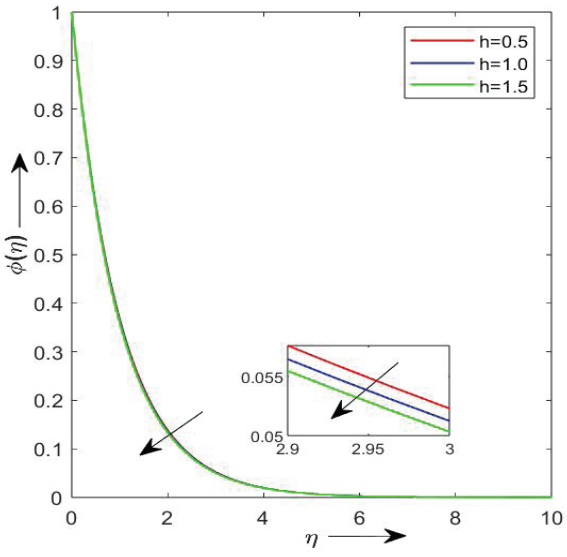

Figure 27. $\phi(\eta)$ vs h.

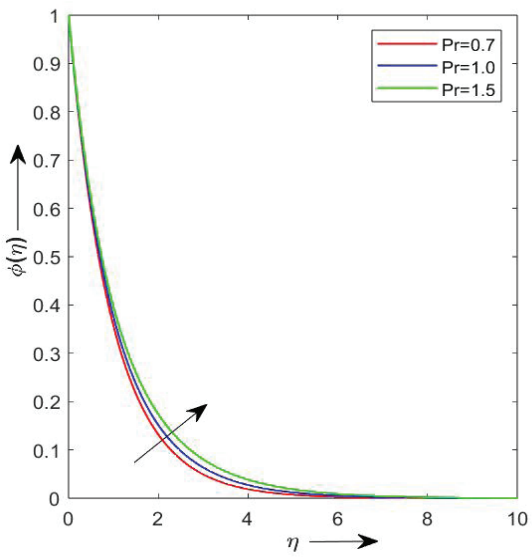

Figure 28. $\phi(\eta)$ vs Pr.

decreases as Hall parameter values increase. A crossflow in the z-direction is generated by the Hall force, which somewhat but not entirely supports concentration. Due to the CBL thickening, the concentration field in Figure 28 exhibits an increasing trend against Pr. The momentum diffusivity to thermal diffusivity ratio is known as Pr (Prandtl number). In actuality, Prandtl number strengthens the viscous forces, which causes the fluid›s viscosity to naturally rise and improve concentration.

Figure 29 makes it clear that when the thermal radiation parameter N is increased, the species concentration decreases. Reduced molecular activity results from a drop in fluid temperature caused by an increase in thermal radiation. Reduced fluid temperature decreases the thermal flux›s force on the concentration flux. The molecular concentration is lowered as a result. This suggests that thermal radiation has a tendency to detard the fluid›s species concentration. Figure 30 demonstrates how the non-dimensional

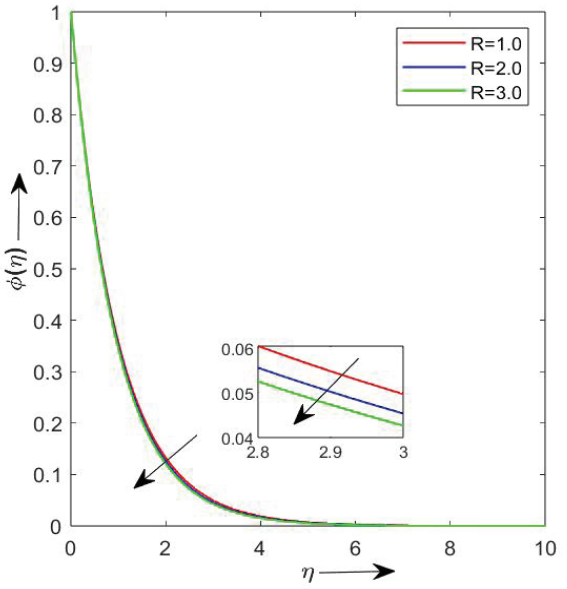

Figure 29. $\phi(\eta)$ vs R.

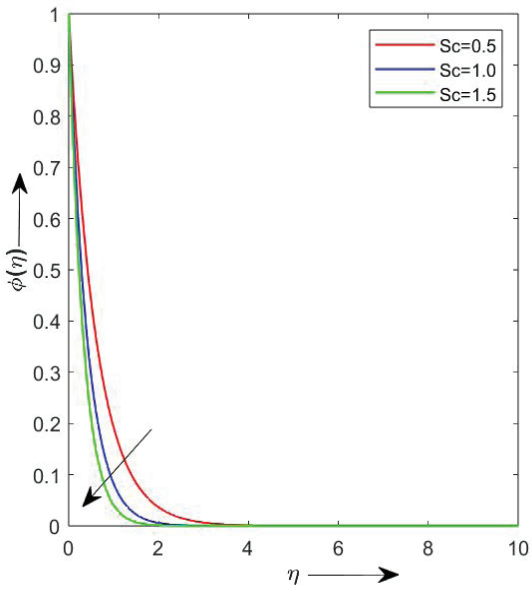

Figure 30. $\phi(\eta)$ vs *Sc*.

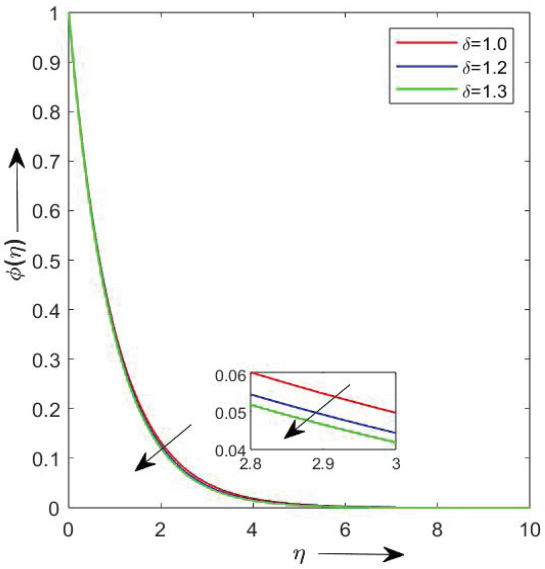

Figure 31. $\phi(\eta)$ vs δ.

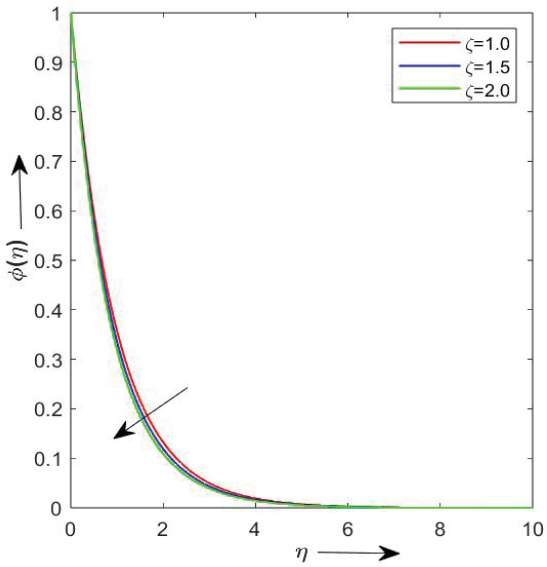

Figure 32. $\phi(\eta)$ vs ζ.

$\phi(\eta)$ falls with changing Sc. The ratio of the viscosity and CBL thicknesses is characterized by Sc (Schmidt number), which is a crucial parameter in the mass transfer process. The CBL is greatly diminished by rise in Sc. A tiny induced flow moves along the sheet surface as a result of the solutal buoyancy effect, which is caused by this drop in solute concentration.

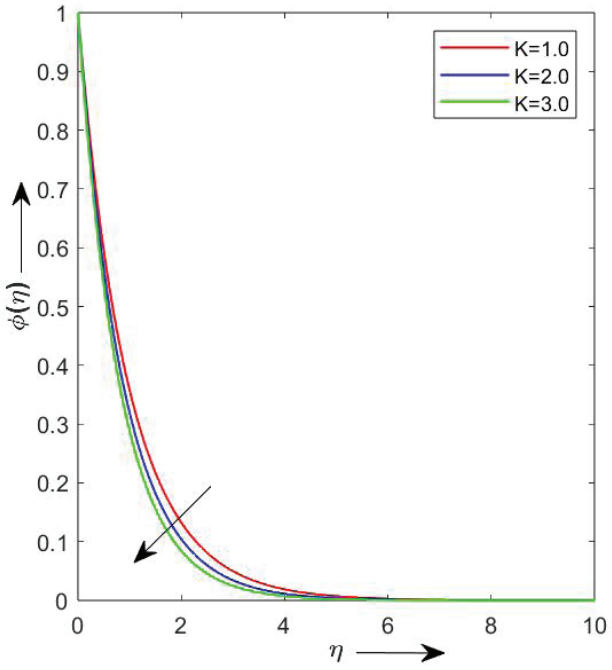

Figure 33. $\phi(\eta)$ vs K.

Figure 31 illustrates, the effect of δ on $\phi(\eta)$. It can be noticed that as δ escalates, $\phi(\eta)$ escalates. It can be observed from Figure 32 that when ζ values increase, the concentration drops. This can be attributed to the fluid›s acceleration caused by positive values of ζ, which lowers the CBL.

The impact of K on $\phi(\eta)$ is depicted in Figure 33. Concentration distributions are shown to decrease as the chemical reaction intensifies. Chemical reactions occur physically with several disruptions. This as a result leads to high molecular mobility, which diminishes the concentration distributions of fluid flow by increasing the transport phenomena.

Table 3 shows the sequel of various fluid flow parameters on the coefficient of skin friction along x-axis $f''(0)$ It can be noticed that the magnitude of $f''(0)$ escalates with the escalating values of H, Sp, Pr, Sc and K . Whereas, decreases with the rise in Bu, h, δ, ζ, Ec and R. Table 3 also shows the sequel of various fluid flow parameters on the coefficient of skin friction along z-axis $g'(0)$. It can be noticed that magnitude of $g'(0)$ accelerates with the rise in Bu, H, ζ, Ec, R and δ. Whereas, decreases with the rise in h, Sp, Pr, Sc and K.

Table 4 shows the sequel of various fluid flow parameters on the rate of heat transfer $\theta'(0)$. It can be contemplated that the magnitude of $\theta'(0)$ escalates with the rise in Bu, h, ζ and Pr. Whereas, decreases with the rise in H, Ec, Sp, R, Sc, δ and K. Table 4 also shows the sequel of various fluid flow parameters on rate of mass transfer $\phi'(0)$ It is demonstrated that magnitude of $\phi'(0)$ escalates with the rise in Bu, h, ζ, Ec, R, Pr, δ and K. Whereas, decreases with the rise in H, Sp and Pr.

Table 3. Variation of skin friction coefficients $f''(0)$ and $g'(0)$ for the various parameters

Bu	H	h	ζ	Ec	Sp	R	K	Pr	Sc	δ	$f''(0)$	$g'(0)$
0.5	1.0	2.0	1.0	0.5	0.5	1.0	1.0	0.71	0.22	1.0	-0.1126	0.2512
0.7											-0.0741	0.2580
1.0											-00187	0.2674
0.5	1.0										-0.1673	0.2512
	1.5										-0.1956	0.3625
	2.0										-0.2245	0.4645
	1.0	2.0									-0.1126	0.2512
		3.0									-0.1009	0.1955
		4.0									-0.0959	0.1557
		2.0	1.0								-0.1126	0.2512
			1.2								-0.0520	0.2625
			1.5								-0.0327	0.2774
			1.0	0.5							-0.1126	0.2512
				1.0							-0.1105	0.2521
				1.5							-0.1084	0.2531
				0.5	0.5						-0.1234	0.2424
					1.0						-0.1739	0.2055
					1.5						-0.2185	0.1775
					0.5	1.0					-0.1126	0.2512
						2.0					-0.0955	0.2588
						3.0					-0.0852	0.2635
						1.0	1.0				-0.1126	0.2512
							2.0				-0.1163	0.2502
							3.0				-0.1194	0.2493
							1.0	0.7			-0.1405	0.2520
								1.5			-0.2100	0.2106
								2.0			-0.2332	0.1995
								0.71	0.5		-0.1301	0.2465
									1.0		-0.1459	0.2429
									1.5		-0.1550	0.2410
									0.22	1.0	-0.1126	0.2512
										1.5	-0.0815	0.2698
										2.0	-0.0440	0.2872

CONCLUSION

A viscous, incompressible, electrically conducting fluid is transferred through an exponentially stretched sheet submerged in a porous material by MHD mixed convection flow, which transfers mass and heat. The impacts of Hall current, Heat source, Joule heating, radiation and chemical reaction are investigated. The bvp4c technique was utilized to provide numerical discussions for the governing equations. A thorough collection of graphics is provided, together with a discussion of how these variables depend on various physical parameters, for the fluid tangential, cross flow velocity, fluid temperature and species concentration.

The following are noteworthy findings:

- The tangential velocity escalates with the rise in Bu, h and ζ. Whereas, it detards with the rise in H, Pr and Sp.
- The cross flow velocity escalates with the rise in H, h and Pr. Whereas, it detards with the rise in Bu, ζ and Sp.
- The temperature profile escalates with the rise in H, Ec, R, δ, Sc and K. Whereas, it detards with the rise in Bu, h, Pr and ζ.
- The concentration profile escalates with the rise in H and Pr. Whereas, it detards with the rise in Bu, h, R, Sc, δ, ζ and K.
- The magnitude of local skin friction coefficient along x- direction escalates with the rise in H, Sp, Pr, Sc and K.

Table 4. Variation of rate of heat transfer and mass transfer coefficients i.e., $\theta'(0)$ and $\phi'(0)$ for the various parameters

Bu	**H**	**h**	**ζ**	**Ec**	**Sp**	**R**	**K**	**Pr**	**Sc**	**δ**	$\theta'(0)$	$\phi'(0)$
0.5	1.0	2.0	1.0	0.5	0.5	1.0	1.0	0.71	0.22	1.0	-0.7552	-1.0480
0.7											-0.7877	-1.0661
1.0											-0.8328	-1.0916
0.5	1.0										-0.7552	-1.0480
	1.5										-0.7218	-1.0400
	2.0										-0.6854	-1.0314
		2.0									-0.7552	-1.0480
		3.0									-0.7824	-1.0542
		4.0									-0.7942	-1.0570
			1.0								-0.7552	-1.0480
			1.2								-0.8188	-1.0777
			1.5								-0.8967	-1.1175
				0.5							-0.7552	-1.0480
				1.0							-0.7374	-1.0499
				1.5							-0.7194	-1.0518
					0.5						-0.7408	-1.0420
					1.0						-0.6700	-1.0145
					1.5						-0.6010	-0.9900
						1.0					-0.7552	-1.0480
						2.0					-0.5870	-1.0629
						3.0					-0.4952	-1.0720
							1.0				-0.7552	-1.0480
							2.0				-0.7482	-1.1568
							3.0				-0.7428	-1.2548
								0.7			-0.7442	-1.0493
								1.5			-1.3948	-0.9810
								2.0			-1.6947	-0.9599
								0.71	0.5		-0.7267	-1.6452
									1.0		-0.7076	-2.4201
									1.5		-0.6987	-3.0473
									0.22	1.0	-0.7552	-1.0480
										1.5	-0.5579	-1.0794
										2.0	-0.3076	-1.1136

Whereas, it decreases with the rise in Bu, h, δ, ζ, Ec and R.

- The magnitude of local skin friction coefficient along z-direction escalates with the rise in Bu, ζ, h, Ec, Sp, R and δ. Whereas, it decreases with the rise in H, Pr, Sc and K.
- The magnitude of rate of heat transfer increases with the rise in Bu, h, ζ and Pr. Whereas, it decreases with the rise in H, Ec, Sp, R, Sc, δ and K.
- The magnitude of rate of mass transfer increases as Bu, h, ζ, Ec, R, Pr, δ and K escalates. Whereas, it decreases with the rise in H, Sp and Pr.

Future work on the problem's irregular behavior and its relationship to thermophoresis and activation energy should be the main focus of the present inquiry. Furthermore, the study of entropy optimization in the magnetohydrodynamic flow of viscous liquids is of tremendous theoretical and technical significance. Metallic coating, crystal growth, electromagnetic pumps, power generators, MHD accelerators, and reactor cooling are just a few examples of the numerous industrial and technological applications where significant effects of hall current, thermal radiation, heat source, and chemical reaction parameters can be found on flow profiles. The production of paper, suspensions, heat exchanger technology, material processing, drying, and surface evaporation of water bodies are only a few of the possible uses for the study's findings. Furthermore, we have taken into account a

conventional fluid instead of a hybrid nanofluid or a nanofluid that has a higher mass transfer and heat efficiency than the fluid under consideration. Since we have left them open-ended for our research's future direction.

NOMENCLATURE

C_p	Specific heat at constant pressure, (J/kgK)
$K^\star$	Rate of first order chemical reaction
f	Dimensionless stream function
g	Cross flow velocity
Ec	Eckert number
q_r	radiative heat flux, (W/m^2)
k_1	Permeability of porous medium, (m^2)
k	Absorption coefficient
H	Magnetic parameter
Pr	Prandlt number
Sp	Porosity parameter
R	Radiation parameter
Gr	Grashoff number
D	mass diffusivity
Sc	Schmidt number
Q	Heat source
h	Hall parameter
Re	Reynolds number
Nu	Nusselt number
Sh	Sherwood number
K	Chemical reaction parameter
Bu	Buoyancy ratio parameter
t	Dimensionless time, (K)
T	fluid's temperature, (K)
g_1	acceleration due to gravity,
C	Species concentration, (kg/m^3)
u	fluid's velocity through x-axis, (m/s)
v	fluid's velocity through y-axis, (m/s)
w	fluid's velocity through z-axis, (m/s)

Greek Symbols

ρ	fluid's density, (kg/m^3)
μ	fluid's viscosity, (Pa s)
σ	Electrical conductivity, ($1/\Omega m$)
η	Dimensionless similarity variable
ν	Kinematic viscosity, (m^2/s)
κ	Thermal conductivity, (W/mK)
α	Thermal diffusivity, (m^2/s)
β_t	Coefficient of thermal expansion
β_c	Coefficient of spatial expansion
ψ	Stream function
τ	Skin friction
θ	Dimensionless temperature
δ	Heat souce parameter
ζ	mixed convection parameter
ϕ	Dimensionless concentration

Superscript

'	Derivative w.r.t η

Subscript

w	Properties at the plate
∞	Free stream condition

Abbreviation

VBL	Velocity boundary layer
TBL	Temperature boundary layer
CBL	Concentration boundary layer

ACKNOWLEGDEMENT

The Department of Mathematics, Cotton University was the site of this research. All of the reviewers' insightful recommendations and remarks are also appreciated by the authors.

AUTHORSHIP CONTRIBUTIONS

Authors equally contributed to this work.

DATA AVAILABILITY STATEMENT

The authors confirm that the data that supports the findings of this study are available within the article. Raw data that support the finding of this study are available from the corresponding author, upon reasonable request.

CONFLICT OF INTEREST

The author declared no potential conflicts of interest with respect to the research, authorship, and/or publication of this article.

ETHICS

There are no ethical issues with the publication of this manuscript.

REFERENCES

[1] Chteoui R, Lotfy K, El-Bary AA, Allan MM. Hall current effect of magnetic-optical-elastic-thermal-diffusive non-local semiconductor model during electrons-holes excitation processes. Crystals 2022;12:1680. [CrossRef]

[2] Crescentini M, Syeda SF, Gibiino GP. Hall-effect current sensors: Principles of operation and implementation techniques. IEEE Sens J 2021;22:10137–10151. [CrossRef]

[3] Kang S. Application of Hall Effect in semiconductor material. Adv Mater Res 2014;986:21–24. [CrossRef]

[4] Midgley D. Recent advances in the Hall Effect: Research and application. Adv Electron Electron Phys 1975;36:153–194. [CrossRef]

[5] Ali FM, Nazar R, Arifin NM, Pop I. Effect of Hall current on MHD mixed convection boundary layer flow over a stretched vertical flat plate. Meccanica 2011;46:1103–1112. [CrossRef]

[6] Kameswaran PK, Narayana M, Sibanda P, Makanda G. On radiation effects on hydromagnetic Newtonian liquid flow due to an exponential stretching sheet. Bound Value Probl 2012;2012:1–16. [CrossRef]
[7] Mandal IC, Mukhopadhyay S. Heat transfer analysis for fluid flow over an exponentially stretching porous sheet with surface heat flux in porous medium. Ain Shams Eng J 2013;4:103–110. [CrossRef]
[8] Singh V, Agarwal S. MHD flow and heat transfer for Maxwell fluid over an exponentially stretching sheet with variable thermal conductivity in porous medium. Therm Sci 2014;18:599–615. [CrossRef]
[9] Jaber KK. Effect of Hall currents and variable fluid properties on MHD flow past stretching vertical plate by the presence of radiation. J Appl Math Phys 2014;2:888–902. [CrossRef]
[10] Khidir A, Sibanda P. Effect of temperature-dependent viscosity on MHD mixed convective flow from an exponentially stretching surface in porous media with cross-diffusion. Spec Top Rev Porous Media 2014;5:157–170. [CrossRef]
[11] Gorla RSR, Gireesha BJ, Singh B. MHD flow and heat transfer of dusty nanofluid embedded in porous medium over an exponentially stretching sheet. J Nanofluids 2015;4:449–460. [CrossRef]
[12] Hayat T, Shafiq A, Alsaedi A, Shahzad SA. Unsteady MHD flow over exponentially stretching sheet with slip conditions. Appl Math Mech 2016;37:193–208. [CrossRef]
[13] Eid MR. Chemical reaction effect on MHD boundary-layer flow of two-phase nanofluid model over an exponentially stretching sheet with a heat generation. J Mol Liq 2016;220:718–725. [CrossRef]
[14] Srinivasacharya D, Jagadeeshwar P. MHD flow with Hall current and Joule heating effects over an exponentially stretching sheet. Nonlinear Eng 2017;6:101–114. [CrossRef]
[15] Govindarajan A, Vijayalakshmi R. Hall current effect in MHD oscillatory couple stress dusty fluid through an inclined saturated permeable channel. Int J Eng Technol 2018;7:801–805. [CrossRef]
[16] VeeraKrishna M, Subba Reddy G, Chamkha AJ. Hall effects on unsteady MHD oscillatory free convective flow of second grade fluid through porous medium between two vertical plates. Phys Fluids 2018;30:023106. [CrossRef]
[17] VeeraKrishna M, Chamkha AJ. Hall effects on unsteady MHD flow of second grade fluid through porous medium with ramped wall temperature and ramped surface concentration. Phys Fluids 2018;30:053101. [CrossRef]
[18] Sarma D, Pandit KK. Effects of Hall current, rotation and Soret effects on MHD free convection heat and mass transfer flow past an accelerated vertical plate through a porous medium. Ain Shams Eng J 2018;9:631–646. [CrossRef]
[19] Rajput US, Kanaujia N. Effects of Hall current on MHD flow past a rotating inclined plate with heat transfer and mass diffusion. Int J Sci Res Math Stat Sci 2018;5:253–258.
[20] Rajput US, Kumar G. Rotation and radiation effects on MHD flow past an inclined plate with variable wall temperature and mass diffusion in the presence of Hall current. Appl Appl Math 2018;13:31. [CrossRef]
[21] Reddy PS, Sreedevi P. MHD boundary layer heat and mass transfer flow of nanofluid through porous media over inclined plate with chemical reaction. Multidiscip Model Mater Struct 2021;17:317–336. [CrossRef]
[22] Goud BS, Bindu P, Srilatha P, Krishna YH. The Joule heating effect on MHD natural convective fluid flow in a permeable medium over a semi-infinite inclined vertical plate in the presence of the chemical reaction. IOP Conf Ser Mater Sci Eng 2020;993:012111. [CrossRef]
[23] Sandhya A, Reddy GR, Deekshitulu GVSR. Steady on MHD heat and mass transfer flow of an inclined porous plate in the presence of radiation and chemical reaction. J Phys Conf Ser 2019;1344:012002. [CrossRef]
[24] Bharathi V, Vijayaragavan R, Prakash J. Heat and mass transfer effect of a magnetohydrodynamic Casson fluid flow in the presence of inclined plate. Indian J Pure Appl Phys 2021;59:28–39.
[25] Dwivedi N, Singh AK. Transient free convective hydromagnetic flow in an infinite vertical cylinder with Hall current and heat source/sink. Heat Transf 2020;49:4091–4108. [CrossRef]
[26] Dwivedi N, Kumar Singh A. Influence of Hall current on hydromagnetic natural convective flow between two vertical concentric cylinders in presence of heat source/sink. Heat Transf 2020;49:1402–1417. [CrossRef]
[27] Jeevitha S, Chitra M, Rushi Kumar B. MHD flow in a rotating vertical cone through a porous medium. Heat Transf 2023;52:2165–2185. [CrossRef]
[28] Tasnim S, Mitra A, Saha H, Islam MQ, Saha S. MHD conjugate natural convection and entropy generation of a nanofluid filled square enclosure with multiple heat-generating elements in the presence of Joule heating. Results Eng 2023;17:100993. [CrossRef]
[29] Zainal NA, Nazar R, Naganthran K, Pop I. Viscous dissipation and MHD hybrid nanofluid flow towards an exponentially stretching/shrinking surface. Neural Comput Appl 2021;33:11285–11295. [CrossRef]
[30] Abbas S, Nazar M, Nisa ZU, Amjad M, Din SME, Alanzi AM. Heat and mass transfer analysis of MHD Jeffrey fluid over a vertical plate with CPC fractional derivative. Symmetry 2022;14:2491. [CrossRef]
[31] Swarnalathamma BV, Babu DP, Krishna MV. Hall current effects on MHD flow of chemically reacting fluid through a porous medium with heat source. Heat Transf 2022;51:4123–4142. [CrossRef]

[32] Sheri SR, Peesu M, Mamidi Narsimha R. Hall current, chemical reaction, and radiation results on transient magnetohydrodynamic flow past an inclined plate: FEM. Heat Transf 2022;51:1876–1899. [CrossRef]

[33] Pati AK, Misra A, Mishra SK, Mishra S, Sahu R, Panda S. Computational modelling of heat and mass transfer optimization in copper water nanofluid flow with nanoparticle ionization. JP J Heat Mass Transf 2023;31:1–18. [CrossRef]

[34] Bishnoi J, Kumar S. Hall current induced MHD convection of a nanofluid subjected to the heat and salt diffusion. Fluid Dyn 2023;58:1169–1182. [CrossRef]

[35] Venthan SM, Kumar PS, Kumar SS, Sudarsan S, Rangasamy G. A computational study of the impact of fluid flow characteristics on convective heat transfer with Hall current using the MHD non-Newtonian fluid model. Chem Eng Res Des 2024;203:789–799. [CrossRef]

[36] Ali A, Khan HS, Noor I, Pasha AA, Irshad K, Al Mesfer MK, et al. Hall effects and Cattaneo–Christov heat flux on MHD flow of hybrid nanofluid over a varying thickness stretching surface. Mod Phys Lett B 2024;38:2450130. [CrossRef]

[37] Elsaid EM, Abdel-Wahed MS. Thermal evaluation of MHD boundary-layer flow of hybridity nanofluid via a 3D sinusoidal cylinder. ZAMM 2024;104:e202300186. [CrossRef]

[38] Nield DA, Bejan A. Convection in porous media. 2nd ed. New York: Springer; 1992. p. 12. [CrossRef]

[39] Kaviany M. Principal of heat transfer in porous media. New York: Springer; 1991. p. 52. [CrossRef]

[40] Shaw S, Guerrero D. Exploring the utilization of Newtonian fluids in heat transfer applications. J Fluid Flow 2023;10:120–130. [CrossRef]

[41] Jerhot J, Šnejdar V. Hall effect in polycrystalline semiconductors. Thin Solid Films 1978;52:379–395. [CrossRef]

[42] Cramer KR, Pai SI. Magnetofluid dynamics for engineers and applied physicists. New York: McGraw-Hill Book Company; 1973. [CrossRef]

[43] Shampine LF, Kierzenka J, Reichelt MW. Solving boundary value problems for ordinary differential equations in MATLAB with bvp4c. Tutorial Notes 2000;1–27.

[44] Wahid NS, Arifin NM, Khashi'ie NS, Pop I, Bachok N, Hafidzuddin MEH. Unsteady mixed convective stagnation point flow of hybrid nanofluid in porous medium. Neural Comput Appl 2022;34:14699–14715. [CrossRef]

[45] Magyari E, Keller B. Heat and mass transfer in the boundary layers on an exponentially stretching continuous surface. J Phys D Appl Phys 1999;32:577–585. [CrossRef]

[46] Ishak A. MHD boundary layer flow due to an exponentially stretching sheet with radiation effect. Sains Malays 2011;40:391–395.